Role of MR Imaging in Head and Neck Squamous Cell Carcinoma

Ahmed Abdel Khalek Abdel Razek, MD[a,†], Nermeen A. Elsebaie, MD[b], Omneya A. Gamaleldin, MD[b], Amro AbdelKhalek, MD[c], Suresh K. Mukherji, MD, MBA, FACR[d,*]

KEYWORDS

• Head and neck cancer • Squamous cell carcinoma • MR imaging • Diffusion • Perfusion • Staging

KEY POINTS

- Squamous cell carcinoma is the most common tumor in the head and neck region.
- Routine precontrast and postcontrast studies are used for the initial evaluation of patients with head and neck cancer.
- MR imaging is important for locoregional spread and staging of head and neck cancer.
- Advanced MR imaging such as diffusion-weighted imaging and perfusion MR imaging are used for initial diagnosis and follow-up of patients with head and neck cancer.
- Imaging is important for the detection of recurrent tumors and monitoring patients after therapy.

BASIC BACKGROUND

Squamous cell carcinoma (SCC) accounts for about 95% of all cancers in the head and neck (HN) region and is the sixth most common cancer worldwide. It can originate from the mucosal epithelial lining of the oral cavity, pharynx, larynx, and sinonasal tract or the skin. Different risk factors lie behind the development of head and neck squamous cell carcinoma (HNSCC) including tobacco and alcohol consumption, exposure to environmental pollutants as well as viral infections namely human papillomavirus (HPV) and Epstein Bar virus (EBV). Infection with HPV is increasingly recognized as a common risk factor for HNSCC mainly arising in the oropharynx. More than 70% of oropharyngeal cancers are associated with an HPV infection with HPV-16 being the primary causative subtype. EBV is a known risk factor for HNSCC arising from the nasopharynx. Currently, significant changes have been made to the WHO classification of HNSCC based on HPV or EBV tumor status. HNSCC is generally more common in men, about 3 to 6 times more than women. The median age of diagnosis for nonvirally associated HNSCC is 66 years. HPV-associated oropharyngeal cancer and Epstein–Barr virus (EBV)-associated nasopharyngeal cancer can present at a relatively younger age, with the median age of diagnosis is about 53 and 50 years, respectively.[1–5]

HNSCC can originate from subsites within the oral cavity (44%), larynx (31%), or pharynx (25%). Clinical presentation of HNSCC varies according to the site of the primary tumor. Cancers of the oral cavity classically present early with a nonhealing ulcer and so they usually present at an early stage. Primary tumors of the oropharynx typically become symptomatic at a later stage, because of their hidden anatomic location. Symptoms include

[a] Department of Diagnostic Radiology, Mansoura University, Elgomheryia Street, Mansoura 35512, Egypt; [b] Department of Radiology, Alexandria Faculty of Medicine, Champollion Street, El-Khartoum Square, El Azareeta Medical Campus, Alexandria 21131, Egypt; [c] Internship at Mansoura University Hospital, Mansoura Faculty of Medicine, 60 Elgomheryia Street, Mansoura 35512, Egypt; [d] Marian University, Head and Neck Radiology, ProScan Imaging, Carmel, IN, USA
[†] Deceased
* Corresponding author.
E-mail address: sureshmukherji@hotmail.com

Magn Reson Imaging Clin N Am 30 (2022) 1–18
https://doi.org/10.1016/j.mric.2021.08.001

dysphagia, odynophagia, or otalgia. Patients with HPV-related cancers of the oropharynx most commonly present with a new, painless level II (lymph nodes [LNs] at the upper jugular level) neck mass and an asymptomatic primary tumor. Patients with cancers of the larynx frequently present with hoarseness of voice, resulting in diagnosis at an early stage. If tumors are neglected, patients can present with dyspnea and airway obstruction prompting tracheostomy. In patients with tobacco-related HNSCC, the risk of a second tobacco-related primary tumor is significantly high, whether synchronous or metachronous, and can be localized at other sites in the HN region, or remotely in the esophagus or lungs.[3–10]

MR IMAGING TECHNIQUE

Routine MR Imaging Sequences

MR imaging offers better contrast resolution than computed tomography (CT) that helps to tumor margins from surrounding tissues. In addition, tumors appearing minimally enhancing on CT will be more evident on MR imaging because MR imaging is more sensitive to contrast enhancement. MR imaging is also more sensitive in the evaluation of perineural tumor spread, intracranial extension, and bone marrow infiltration. Conventional MR imaging sequences to assess HNSCC should include a T1 without fat suppression, T2 with and without fat suppression, and T1 postcontrast with fat suppression. These sequences are used to analyze certain characteristics of the primary tumor and possible nodal involvement.[6–9] Precontrast T1-weighted sequences should be performed without fat saturation for identification of the fat planes and delineation of normal anatomy. T2-weighted sequences should be acquired with fat suppression to increase the conspicuity of pathologic processes which often have increased T2 signal. The use of fat suppression on postcontrast T1-weighted sequence also maximizes the conspicuity of enhancement, because enhancing tissues may otherwise be the same signal intensity as surrounding fat. This technique is particularly important in the detection of perineural spread and for skull base involvement. Fat suppression for postcontrast T1 also increases the conspicuity of nodal necrosis and extranodal extension (ENE) of tumor which is currently added in the nodal staging for all tumors except nasopharyngeal carcinoma and HPV/p16 positive oropharyngeal tumors.[10–13] Some problems cannot be solved by anatomic sequences alone. Post-therapy changes such as inflammation and fibrosis show overlapping signal characteristics with recurrent or residual tumors. For LN assessment, the reactive LN that can be enlarged similar to nodal metastasis and normal-sized nodes can still contain tumors.[11–14]

Diffusion-Weighted Imaging

Routine diffusion-weighted imaging

Diffusion-weighted imaging (DWI) measures cellular density and cytoarchitecture by assessing water diffusivity. DWI is used in HN to differentiate SCC from lymphoma, diagnose LN metastasis, and differentiate recurrent neoplastic lesions from post-radiotherapy and chemotherapy changes. DWI is also able to detect changes in tumor prior size changes on anatomic sequences become visible, which can help to predict the early effect of treatment.[15–18]

Diffusion tensor imaging

Diffusion tensor imaging reflects micromovement of water molecules and can distinguish between different tissue compartments at the cellular level with different matrices. The most common metrics of diffusion tensor imaging used are mean diffusivity and fractional anisotropy (FA). Cellular tumors have a small extracellular space with low diffusivity and high anisotropy giving high FA values. Diffusion tensor imaging can be used in the HN to differentiate malignant from benign HN lesions, and can help prediction of recurrent HNSCC after treatment.[19,20]

Diffusion kurtosis imaging

The conventional DWI assess considers only water diffusion in one compartment which is the extracellular compartment. In diffusion kurtosis imaging, the interaction of water molecules with cell membranes is also considered. To estimate this motion, it is necessary to acquire b-values above 2000 mm^2/s. The main parameter derived from diffusion kurtosis imaging is the mean kurtosis (MK), which reflects the heterogeneity of the tissues. Aggressive lesions with higher mitotic index, presence of necrosis, and neoangiogenesis will show higher MK values than less aggressive lesions. However, in order to apply it, it is necessary to acquire multiple b-values and this means a longer examination time, with the consequent motion artifacts inherent to the HN region.[21]

Perfusion-Weighted Imaging

It provides a noninvasive assessment of microvascular characteristics of lesions. There are 3 main sequences of MR perfusion, contrast administration is used in 2 sequences: dynamic contrast-enhanced (DCE) and dynamic susceptibility contrast (DSC) techniques, in the third one, arterial spin labeling (ASL), no contrast administration is required, alternatively magnetically labeled arterial blood water is used as a tracer. DCE MR imaging

and to a much lesser extent ASL are the perfusion techniques used to assess HN tumors.[8–13]

Dynamic contrast-enhanced MR imaging perfusion

It is the most commonly used technique, in which the passage of contrast bolus between the intravascular and extravascular compartments of the lesion is analyzed. An increase in the tissue signal is detected when the contrast reaches the extravascular space; the resulting signal intensity change over time creates the intensity-time curves. Data from this curve can be analyzed semiquantitatively or quantitatively. The semiquantitative method classifies the morphology of the signal intensity curve. The initial enhancement in the first 120 seconds is labeled as rapid, medium, or slow enhancement, and late enhancement beyond 120 seconds is described as persistent, plateau, or shout. In the quantitative method, additional tissue-specific parameters can be estimated including the transfer constant (Ktrans) which reflects the transfer rate of contrast from the plasma into the tissue extracellular space, the volume fraction of the extravascular extracellular space (ve), the volume fraction of plasma in tissue (vp), and the transfer rate from the extravascular extracellular space back to the plasma (kep).[12,22]

Dynamic susceptibility contrast MR imaging

DSC perfusion is based on the inhomogeneity of the magnetic field during the passage of a bolus of contrast through a capillary bed. Mean transit time, blood flow, and blood volume can be calculated. However, this technique is sensitive to motion artifacts because of the voluntary and involuntary movements in the HN region, which affects the reliability of the results. Also, blood products, calcifications, and air result in artificial signal loss.[23,24]

Arterial spin labeling

In ASL, blood flow can be calculated, which could reflect neovascularity within tumors. It is of particular clinical interest because of its relative speed, minimal postprocessing, and avoidance of gadolinium-based contrast agents. The main disadvantage of ASL is the low signal-to-noise ratio.[25–27]

MR Spectroscopy

Proton MR spectroscopy (MRS) is a noninvasive technique that can provide functional information through the evaluation of tissue metabolite concentrations. In HN lesions, the metabolites choline (Cho), creatine (Cr), lipid (Lip), and lactate (Lac) are often evaluated. Spectroscopy should be regarded as complementary to other functional MR imaging techniques in assessing HNSCC.[28]

Artificial Intelligence

Recently, advanced imaging analysis and processing is done with radiomics, deep learning with histogram analysis of quantitative parameters of MR imaging.[29–31]

ROLE OF IMAGING

Tumor Localization

The extent of mucosal involvement by the primary tumor is best assessed by endoscopic evaluation, whereas submucosal and deep extension is better documented at MR imaging. Tumors demonstrate isointense to hypointense signal on T1-weighted images (T1WIs) and hyperintense signal on T2-weighted images (T2WIs) compared to adjacent muscle (**Fig. 1**). Diffusion-weighted MR imaging can help to differentiate HNSCC from adjacent muscles as tumor shows lower apparent diffusion coefficient (ADC) values compared with benign tissue because of its high cellularity (**Fig. 2**). DCE may add benefits in discrimination between malignant

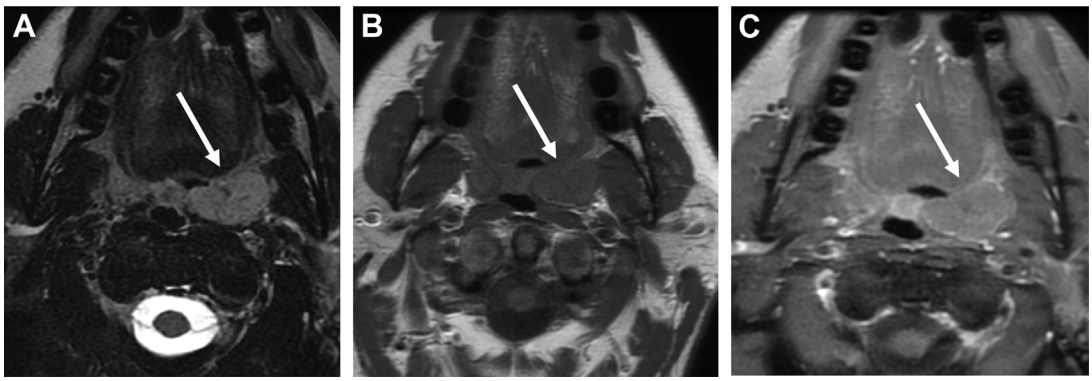

Fig. 1. MR imaging characteristics of squamous cell carcinoma. (*A*) Axial T2WI shows a left tonsillar carcinoma, which is a high signal. The lesion has T1 intermediate signal (*B*) and homogeneously enhances on fat-suppressed contrast-enhanced T1-weighted (T1W) sequences (*C*) (*arrows*).

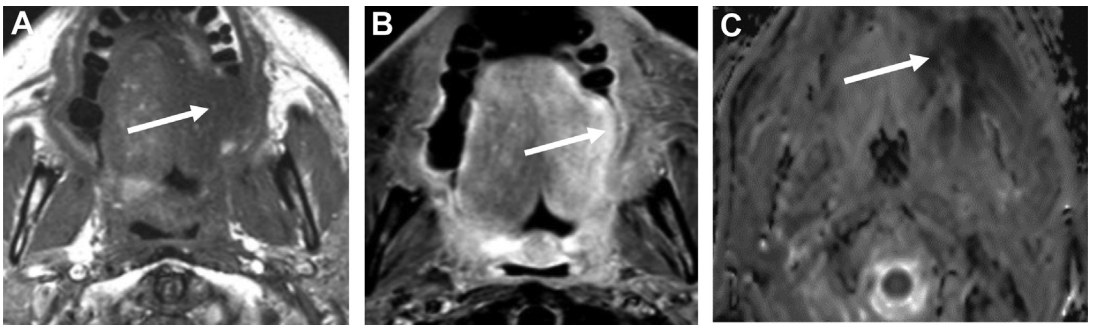

Fig. 2. DWI for identifying recurrent tumor. Noncontrast T1WI was obtained in a patient with a left retromolar trigone carcinoma that had been treated with combined chemotherapy and radiation therapy. (*A*) Axial noncontrast T1WIs show an intermediate signal involving the left retromolar trigone extending anteriorly to involve the posterior left maxillary alveolar ridge (*A*), which enhances following contrast (*B*). These imaging findings are indeterminant; however, the ADC maps show the area to have decreased signal (*C*), which was suspicious for recurrent tumor, and was confirmed with a biopsy (*arrows*).

lesions and adjacent normal tissues. The idea is based on that tumors with increased neoangiogenesis show earlier arrival of the contrast medium compared with normal tissue. Some studies showed that Ktrans, Kep, and Ve values are significantly higher in tumor areas than in the adjacent normal muscle. At MRS, the Cho/Cr ratio is found to be significantly elevated in cancer tissues in comparison with normal neck musculature due to increased cell membrane turnover in the cancer tissue.[7–12]

Locoregional Extension

Submucosal invasion

It is important to evaluate the full local extent of the primary tumor and detect submucosal and deep spread, perineural extension, bone and cartilage invasion, or intracranial involvement. Although there have been many changes in the updated eighth edition of the Cancer Staging Manual of the American Joint Committee on Cancer implemented in January 2018 (AJCC), it is necessary to ensure that all information that alters the tumor stage are included in the report. The location of the primary tumor can influence the selection of the initial imaging modality. MR imaging provides superior soft-tissue contrast is often the preferred imaging modality for evaluating the oral cavity, nasopharyngeal and oropharyngeal tumors. MR imaging can be affected by motion in the region of the larynx because of its relatively long scanning time. On MR imaging, the tumor usually appears hyperintense to muscle on T2WI and hypointense or isointense to muscle on T1WI (see **Fig. 1**).

The precontrast T1WI is particularly useful in differentiating tumor from surrounding fat. When evaluating the primary tumor (T), the specific criteria in the staging tables may require distinction by the size of the tumor or by specific invasion patterns.[32–34]

When measuring tumor size, the longest diameter is used. Conventional sequences can overestimate tumor size if inflammatory changes present. The use of DWI can help to better detect and demonstrate tumors because most squamous cell cancers are relatively hypercellular and can show diffusion restriction. The tumor typically shows an intermediate signal on T2WI and low ADC values at DWI, whereas peritumoral edema expresses a high signal on T2WI and high ADC values. Sometimes, delayed postcontrast T1 volumetric sequences (at least 5 min) may be used to demonstrate ish-out of tumor (which becomes darker) and progressive enhancement of surrounding inflammation (which becomes brighter).[31–35]

Tongue depth of invasion

In oral cavity tumors, of which tongue is the most common subsite, evaluation of the depth of invasion (DOI) is added as a critical determinant of T-staging. It can be measured on T1WIs by measuring the vertical distance between the deepest point of tumor infiltration and the simulated normal mucosal line. Many studies reported that MR imaging–determined DOI greater than 7.5 mm is significantly associated with the presence of neck LN metastasis, which added a nearly 3-fold risk of neck LN metastasis.[32–34,36] However, AJCC staging criteria emphasize that DOI is histologic measurement.

Thyroid and cricoid cartilage invasion

Accurate determination of thyroid cartilage invasion is essential for proper staging of laryngeal and hypopharyngeal cancers as they can upstage tumors to critical points where decision making for offered treatment is between chemoradiation and total laryngectomy. The first-line imaging for these

Fig. 3. CT of laryngeal cartilage invasion. (*A*) Axial CT was obtained through the thyroid cartilage reconstructed in bone algorithms in a patient with an SCCA of the anterior commissure. Cancer has eroded the inner cortex (*long arrow*) but the outer cortex is preserved (*short arrow*) indicating the stage of the tumor is T3. (*B*) Axial CT was obtained through the thyroid cartilage reconstructed in bone algorithms in a patient with an SCCA of the right true vocal cord. Cancer has eroded both the inner cortex (*long arrow*) and outer cortex (*short arrow*), indicating the stage of the tumor is T4.

tumor types is usually CT, which affords an excellent evaluation of these areas without swallowing artifacts in most cases. Tumor extending beyond the external margin of the cartilage ("extralaryngeal") is the most reliable feature of cartilage invasion. CT is able to pick up small defects of the cortical layer, while sclerosis is a nonspecific finding (**Fig. 3**). MR is superior in identifying intracartilaginous penetration: findings of infiltration are the copresence of low T1 (**Figs. 4** and **5**), intermediate T2 signals, and contrast-enhancement. Conversely, a high T2 signal is indicative of intracartilaginous edema, while the contribution of DWI is still not clear.[37,38]

Bone invasion

CT and MR are often used as complementary tools for preoperative planning. CT is more sensitive for demonstration of cortical erosion (**Fig. 6**). MR is better for early marrow invasion which appears as a defect in the low signal intensity of the bone cortex on T1WI and replacement of the high signal intensity marrow by low signal intensity tissue on T1WI with evident enhancement after contrast (**Fig. 7**). Marrow invasion of the mandible in oral cavity tumors will require surgical resection with a segmental mandibulectomy, rather than a marginal mandibulectomy for cortical erosion only. Marrow invasion will be evident on CT if the tumor is seen involving both sides of the mandible with extensive mandibular lytic destruction. When there is a subtle irregularity of the mandible and a critical surgical decision must be made, as to whether there is marrow invasion, MR may be necessary.[39,40]

Prevertebral invasion

The prevertebral space can be invaded by carcinomas of the nasopharynx, oropharynx,

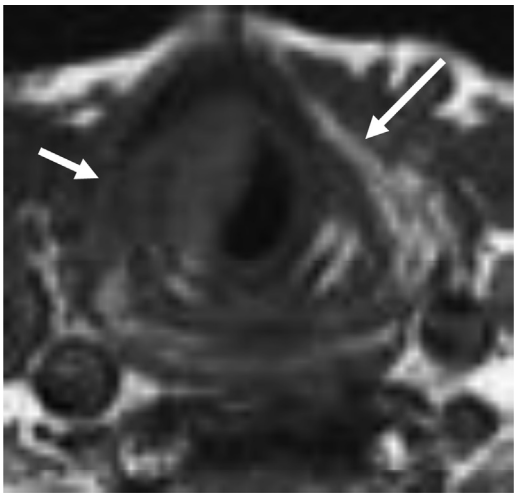

Fig. 4. MR imaging of cartilage invasion. Axial noncontrast T1W sequence was obtained through the thyroid cartilage in a patient with an SCCA of the right true vocal cord. Note the normal high T1W signal within the thyroid cartilage on the left side (*long arrow*) but replacement of the T1W (*short arrow*) adjacent to the tumor. The replacement of the normal T1W signal could be either due to tumoral invasion or peritumoral inflammation.

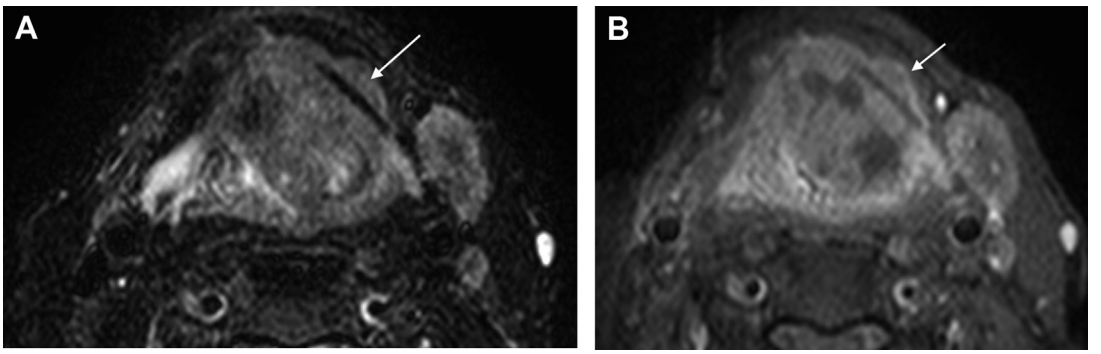

Fig. 5. MR imaging of cartilage invasion. Axial STIR and T1 postcontrast fat-saturated images (*A*, *B*) showing transglottic cancer obstructing the airway and transfixing the left thyroid cartilage (*white arrows*) with intermediate T2 signal and heterogeneous enhancement.

hypopharynx, or rarely larynx. The presence of obvious tumor fixation renders the tumor irresectable as tumor-free surgical margins cannot be achieved. In nasopharyngeal carcinoma, invasion to prevertebral muscles is currently clarified as T2 stage, yet associated with poor prognosis as the likelihood of locoregional recurrence and hematogenous metastases is increased. Several MR imaging signs may suggest the presence of prevertebral space invasion including obliteration of the retropharyngeal fat plane, ipsilateral muscle concavity, and T2 hyperintensity of the adjacent muscle (**Fig. 8**). However, these MR imaging findings are considered unreliable as they can be due to peritumoral edema, without actual muscle invasion. Still, accurate determination of neoplastic fixation to the prevertebral fascia is assessed most accurately intraoperatively during neck dissection or with manual manipulation on endoscopy under general anesthesia. On the contrary, the absence of prevertebral space involvement can be clearly suggested on CT or MR imaging in cases where there is the preservation of the retropharyngeal fat plane.[34,41]

Esophageal invasion

Cervical esophageal invasion is reported in patients with hypopharyngeal cancer. MR imaging shows esophageal wall thickening, effacement of the adjacent fat plane, and T2 signal wall abnormality (**Figs. 9** and **10**). Circumferential mass more than 270° is a specific sign for esophageal invasion of HNSCC.[34,36–42]

Tracheal invasion

MR imaging is the modality of choice for the evaluation of tracheal invasion by thyroid cancer.

Fig. 6. CT findings of bone erosion. (*A*) Axial contrast-enhanced CT shows a right floor of mouth carcinoma (*arrow*). (*B*) Bone algorithm shows erosion of the adjacent lingual cortex (*arrow*).

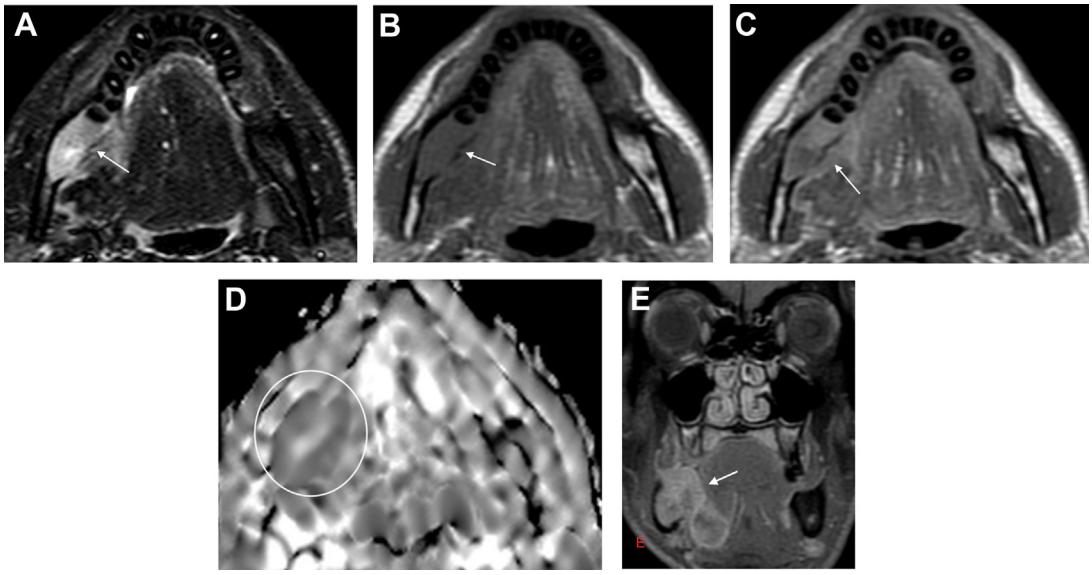

Fig. 7. Bone marrow invasion. Axial STIR (*A*), T1 (*B*), T1 postcontrast (*C*), and ADC map (*D*) of right retromolar trigone cancer showing hypointense mass invading the mandible with cortical erosions, expansion, and marrow replacement (*white arrows*). It shows a low ADC value of 0.9 in the ADC map (*circle*). T1 postcontrast fat-saturated coronal section (*E*) shows the heterogeneous enhancement of the tumor and infiltration of the mandible and floor of the mouth (*white arrow*).

Tracheal invasion is diagnosed by a combination of 3 criteria: tumor abutting circumference of the trachea for 180° or more, an intraluminal mass, or a soft-tissue signal within the cartilage (see **Figs. 9** and **10**). Invasion of the recurrent laryngeal nerve is predicted by the finding of effaced fatty tissue. The accuracy of these criteria is 90%.[43]

Cutaneous invasion

HNSCC may extend into the subcutaneous and cutaneous tissue. Imaging is important for surgical planning for the reconstruction of skin defects. Skin invasion at HNSCC is a bad prognostic sign. The presence of subcutaneous and cutaneous fat invasion appears as low signal intensity on T1WI and high signal on T2WI[44,45]

Perineural spread

It is critical to report this finding as, even if it does not change the tumor stage, it can significantly alter surgical and/or radiation planning. On CT scans, it can appear as a widening of the bony neural foramina at the skull base or at the mandibular or mental foramina of the mandible. MR imaging, with its higher contrast resolution and greater sensitivity to contrast enhancement, has been shown to be more sensitive on T1WIs, and there may be loss of normal fat padding around the nerve at the skull base. Characteristic findings of retrograde perineural are diffuse enhancement of an enlarged nerve (**Fig. 11**). On T2 and contrast-enhanced fat-saturated T1WIs, there is a thickening of the involved nerve. Muscle denervation subsequent to perineural tumor spread may also be evident and is much easier to detect on MR than CT, due to early T2 hyperintensity and contrast enhancement of denervated muscles.[46,47]

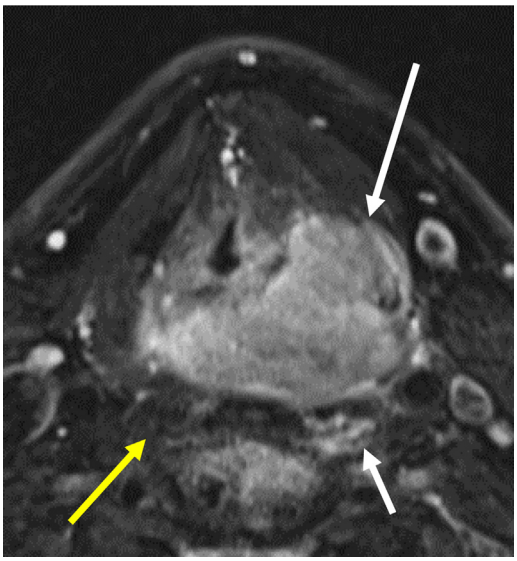

Fig. 8. MR imaging findings suggestive of prevertebral muscle involvement. Axial T2WI obtained in a patient with a large pyriform sinus carcinoma (*long white arrow*) shows increased T2 signal in the ipsilateral longus coli muscle (*short white arrow*), which is suspicious for muscle involvement. Compare this with the normal appearance of the contralateral longus coli muscle (*yellow arrow*).

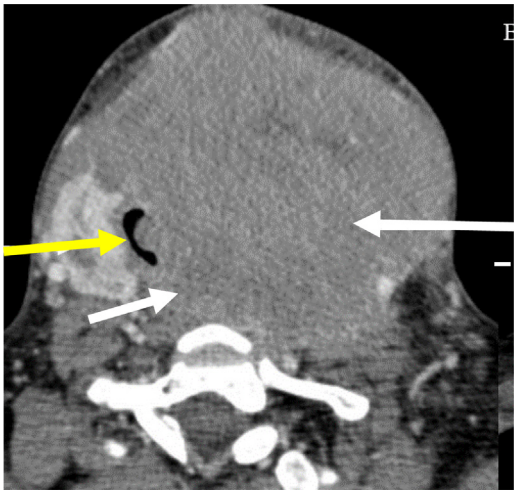

Fig. 9. Esophageal and tracheal invasion. Axial contrast-enhanced CT shows a large mass (*long white arrow*) extending medially to invade the trachea (*yellow arrow*) and extending posteriorly to involve the cervical esophagus (*short white arrow*).

Brachial plexus invasion

Brachial plexus invasion in HNSCC makes the tumor unresectable (Fig. 12). MR imaging shows high signal intensity on T2WI and enhancement along with brachial plexus or scalene muscles.[33,34]

Nodal Metastasis

Detection of nodal metastases in patients with HN cancer is important for treatment planning, the extent of radiation treatment field, or surgical neck dissection method. Morphologically, metastatic LNs should be rounded, with loss of the fatty hilum and more than 10 mm in short axis, focal necrosis may be present (Fig. 13). In addition to size and morphologic criteria, functional MR imaging techniques can add more data to suggest the presence of metastatic LNs, particularly in normal-sized nodes. There are multiple studies that have reported significantly lower ADC in metastatic LNs (Figs. 14 and 15) than that of normal nodes. They suggested average ADC values of 1.02 to 1.38 $\times$ 10^{-3} mm^2/s as a threshold value for differentiating malignant from benign LNs. It has been found that metastatic LNs associated with HPV-positive tumors tend to have lower ADC values on DWI compared with the HPV-negative LN metastasis.[6–10]

Few studies evaluated DCE-MR perfusion in the detection of metastatic LNs. Some studies showed that values of the Ktrans and Ve are found to be higher in metastatic LNs than in benign LNs. The Ktrans stands for the volume transfer constant, which is closely related to the perfusion and integrity of the endothelial cells. The Ve is a symbol of the extravascular extracellular volume fraction. Several studies on DCE MR imaging showed that the Ve is considered as an index of necrosis. Endothelial cells in tumor vessels are often pathologically immature, lacking in pericyte and smooth muscle coverage. Once an LN is invaded by tumor cells, new vessels with high permeability are generated. The increase in the number of new vessels can be detected as increased values of Ktrans of metastatic LNs corresponding to the histopathological changes. On the contrary, other studies showed that metastatic nodes have significantly lower Ktrans than the normal nodes. Such a low level of vascular-related parameters could be explained by necrosis, hypoxia, and elevated interstitial fluid pressure contributing to poor perfusion commonly observed in aggressive tumors.[48,49]

Extranodal extension

The new AJCC8 introduced the clinical ENE designation which is assessed on clinical examination (see Fig. 13). This finding should be looked for in all tumors except nasopharyngeal carcinoma and HPV/p16 positive oropharyngeal tumors. The presence of fixation of the nodal mass to adjacent

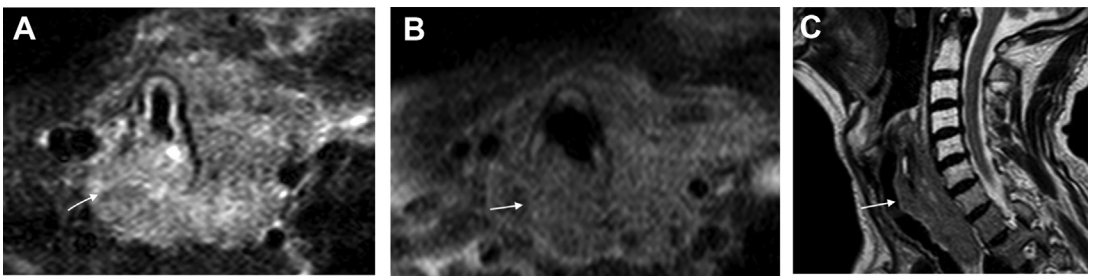

Fig. 10. Esophageal and tracheal invasion: Axial STIR (*A*), T1 postcontrast fat-saturated (*B*), and sagittal T2 (*C*) showing hypopharyngeal cancer invading the cervical esophagus, left thyroid lobe, and cervical trachea (*white arrows*). It shows a hypointense signal in T2 with heterogeneous enhancement.

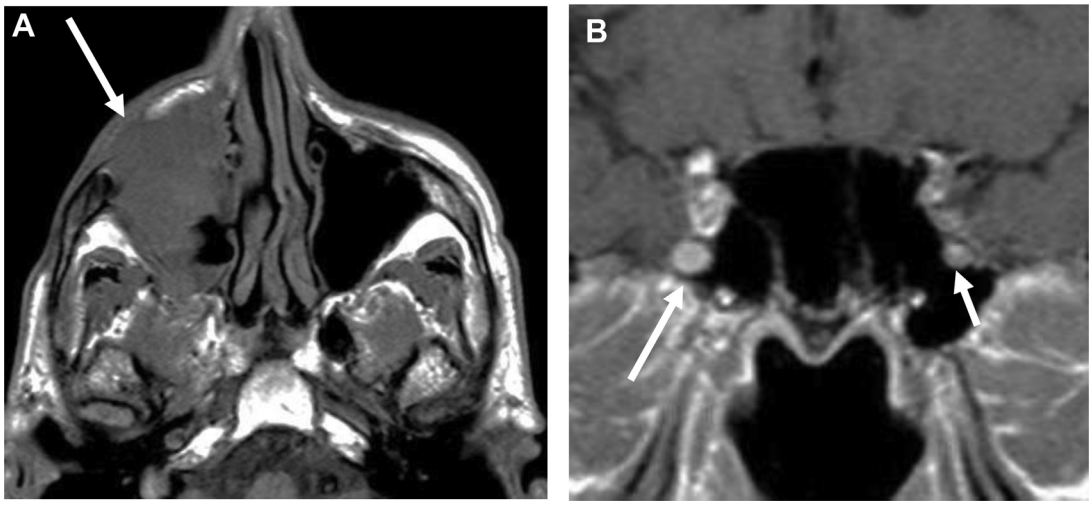

Fig. 11. MR imaging of perineural spread. (*A*) Axial noncontrast T1WI shows a large right maxillary sinus carcinoma (*arrow*). (*B*) Coronal contrast-enhanced T1WI shows diffuse enlargement and enhancement of the maxillary division of the trigeminal nerve (V2) indicative of retrograde perineural spread (*large arrow*). Compare this with the normal appearance of V2 on the contralateral site (*short arrow*).

structures such as skin or muscles or evidence of nerve dysfunction is suggesting the extranodal spread of the tumor, which upgrades the tumor to cN3b designation and grouping of stage IVB. Imaging may provide supportive evidence of this clinical ENE.[33,34]

On CT and MR imaging, different signs suggest the presence of ENE of the tumor. The most reliable imaging feature supporting the clinical diagnosis of ENE is the clear infiltration of perinodal tumor into adjacent fat or muscle. Other CT or MR imaging findings of ENE include indistinct nodal margins, irregular nodal capsular enhancement, and interruption in the nodal capsule. Several additional MR imaging signs have been reported such as the "vanishing border" sign where the fat space between node and adjacent tissues is obliterated on T1WIs, "flare" sign with high signal in interstitial tissues around and extending from the node on fat-suppressed T2WIs, and the "shaggy margin" sign where there is irregular or interrupted enhancement at the periphery of the nodes on axial gadolinium-enhanced T1WIs. Some studies indicated that ENE is more common in the presence of nodal necrosis and in nodes larger than 2 cm, while others find no correlation with nodal size.[50,51]

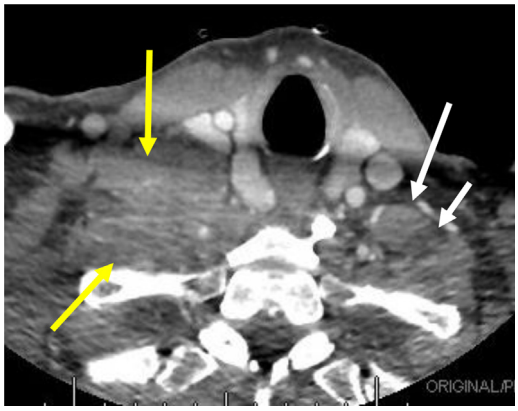

Fig. 12. SCCA invasion of brachial plexus. Axial contrast-enhanced CT shows normal appearance of the left anterior scalene (*long white arrow*) and supraclavicular brachial plexus (*small white arrow*). There is a large mass invading the right brachial plexus characterized by an invasion of the anterior scalene and supraclavicular brachial plexus (*yellow arrows*).

Distant Metastasis

The most common sites of distant metastasis in HNSCC are the lungs, followed by bone and liver. Variable factors increase the incidence of distant metastasis including advanced T-stage, poorly differentiated tumors, bilateral LN metastasis, and presence of ENE. Screening with integrated whole-body flouro deoxyglucose (FDG)-PET/CT including CT scan of the chest is currently the most valuable screening technique. Whole-body MR imaging (WB-MRI) has also become clinically feasible, with substantially reduced examination times. The use of whole-body diffusion-weighted MR imaging has even more advantages over standard anatomic WB-MRI sequences because of higher lesion-to-background contrast without the need for gadolinium contrast. Recently, images obtained with the PET-MR imaging system exhibited detailed resolution and greater image

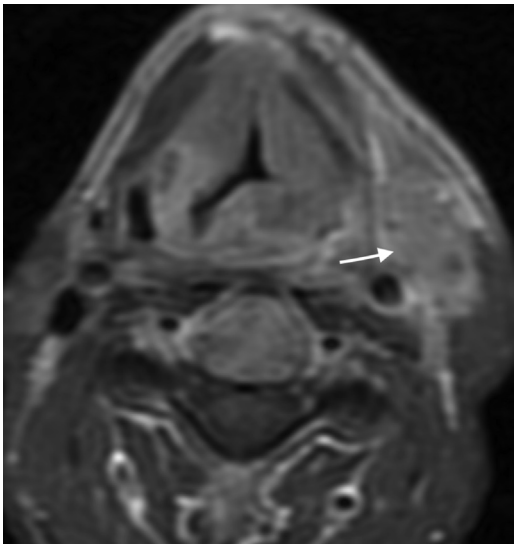

Fig. 13. Metastatic cervical lymph nodes. Axial T1 postcontrast image of a patient with SCC of the larynx showing left level II group metastatic lymph node (*white arrow*). It shows a globular shape, irregular outline, lost hilum, and invasion of left sternomastoid muscle; features of nodal metastases with ENE.

contrast in comparison to those from the PET/CT system, which may further improve detection of distant metastasis.[52,53]

Tumor, Node, Metastases Staging

Many changes have been added to the new AJCC8 for HNSCC. One of the significant changes is the staging of oropharyngeal tumors according to the HPV status. This change is based on the finding HPV-associated oropharyngeal SCC has a markedly better prognosis despite their tendency to have early and extensive nodal metastasis. In the new classification, ipsilateral metastatic nodes are considered as N1, bilateral or contralateral nodes are to be designated as N2, and nodes that are larger than 6 cm are to be designated as N3. The prognostic table of the overall stage group is also changed. Stage I is determined by T1–2 and N0–1, stage II by T1–2 and N2 or T3 and N0–2, and stage III by T4 or N3, whereas stage IV is reserved for patients with metastatic disease. Accordingly, up to 80% of these tumors are classified as stage I. This is in contrast to p16−/non-HPV oropharyngeal SCC where most tumors are stage III or IV at presentation.[34,35]

Another important change regarding metastatic nodal SCCs is adding the pathologic and clinical criterion of ENE. This is applied in all HNSCCs except nasopharyngeal cancer and HPV-associated oropharyngeal cancer. Previously, pathologic diagnosis of ENE is found to be associated with poor prognosis for SCC, but it has not been part of the clinical or pathologic tables until AJCC8. Clinical ENE is suggested by the finding of fixation of the nodal mass to adjacent structures such as skin or muscles or evidence of nerve dysfunction suggesting nerve invasion. The designation of clinical ENE results in cN3b stage, which upstages tumors to stage group IVB. Details about the AJCC 8th classification will be discussed in the next article.[32–35]

Prognostic Parameters

Human papilloma virus

Oropharyngeal SCC has a different biology, and is associated with a better prognosis than HPV. In

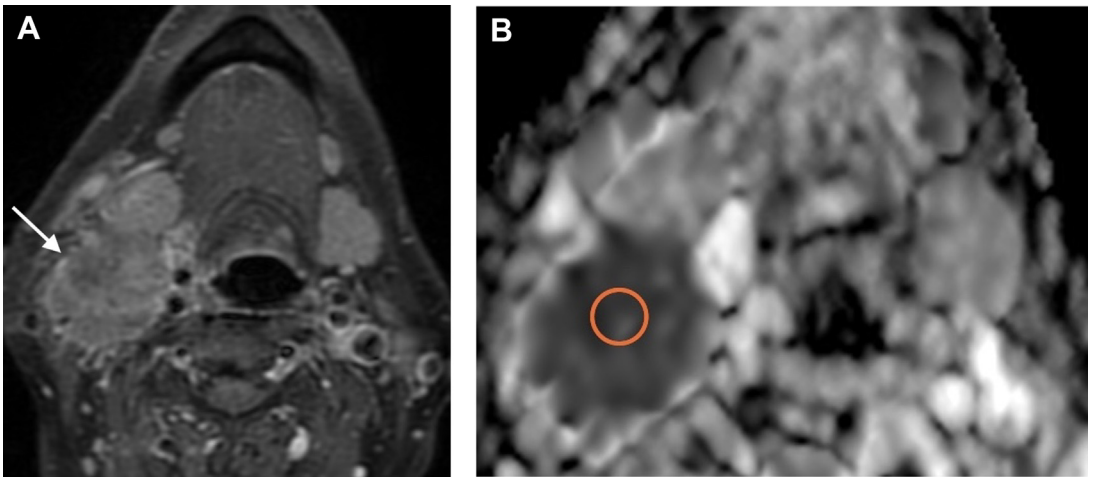

Fig. 14. Metastatic cervical lymph nodes. Axial T1WI (*A*) of a patient with metastatic SCC node shows irregular nodular periparotid lymph node (*white arrow*). In ADC map (*B*), it shows low signal intensity; ADC value 0.9×10^{-3} mm^2/s.

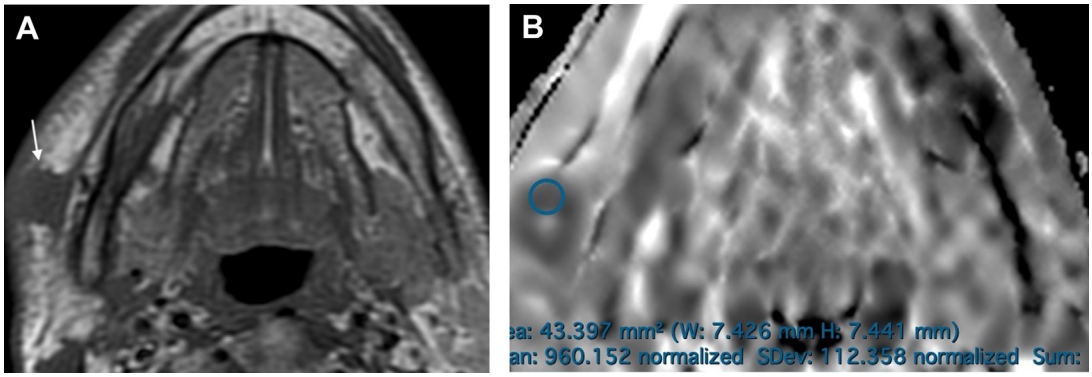

Fig. 15. Lymphomatous cervical LN. Axial T postcontrast fat-saturated image (*A*) showing large level II nodal mass with heterogeneous enhancement and invasion of the submandibular gland (*white arrow*) in a patient with nodal NHL. ADC map (*B*) showing a low signal intensity of the lymph node; ADC value 0.6 $\times$ 10^{-3} mm^2/s.

the AJCC8, the HPV-positive oropharyngeal SCC is staged separately from the HPV-negative type. DWI can offer a noninvasive imaging biomarker for HPV status of oropharyngeal SCC. Recent studies reported a lower mean ADC value in a primary lesion of HPV-positive oropharyngeal SCC compared with the HPV-negative tumors. HPV-negative oropharyngeal SCC showed higher ADC, reflecting histopathological features such as high stromal content, low cellularity, and micronecrosis. These prognostic characteristics likely contribute to the association of pretreatment high ADC values with poor outcomes in patients with HNSCC.[45,46]

Gross target volume

Tumor volume measured at MR imaging is referred to as gross target volume that correlates with local control and outcome for HNC and measure of the response to therapy. Tumor volume appears to be the strongest independent predictor of local failure after radiation therapy.[54]

Degree of differentiation

Differentiation of well-moderately differentiated HNSCC from poorly differentiated HNSCC is important for determining the prognosis and clinical outcome of patients. Some studies mentioned that poorly differentiated tumors may have lower ADC values than well/moderately tumors. Other authors, however, reported that ADC values could not distinguish between them. At histopathology, endothelial cells of poorly differentiated HNSCC are more immature, lacking in pericyte and smooth muscle coverage, these features can be highlighted at DCE. The increased permeability of these new vessels in poorly differentiated HNSCC results in increased values of Ktrans and Ve compared with well-differentiated HNSCC; corresponding to the histopathological changes.[5–25,26–59]

Treatment Planning

Detection of the best site for biopsy

Detection of the best biopsy site of the HN neoplasm is important for the best results. At routine MR imaging, biopsy is better taken from areas of lowest signal intensity at T2WIs and shows contrast enhancement and avoids areas of necrosis. An ADC map can differentiate viable from necrotic regions of malignancy. The viable regions of the tumor show restricted diffusion and necrotic regions display unrestricted diffusion. A biopsy is better when taken from the region of restricted diffusion with the lowest ADC value on the ADC map.[60]

Radiation therapy planning

Cross-sectional imaging has revolutionized radiation therapy planning and treatment effectiveness by allowing for conformational focus of radiation using 3-dimensional plans based on CT or MR imaging. The goal of radiation therapy is to control locoregional disease in the absence of distant metastatic disease. Here the value of adding FDG-PET to CT to detect unsuspected distant metastatic disease is a principal advantage of PET-CT in the evaluation of a patient under consideration for radiation therapy. To optimize conformational treatment plans, the radiation oncologist must know the precise delineation of the primary malignant mass and the extent of locoregional nodal disease (**Fig. 16**). Adding FDG-PET to the currently used CT imaging at simulation is becoming more widespread because of the improved delineation of tumor mass margins and assessment of locoregional tumor spread[60]

Differentiation from Lymphoma

SCC and lymphoma are the most common malignancies in the HN. Differentiation between these 2

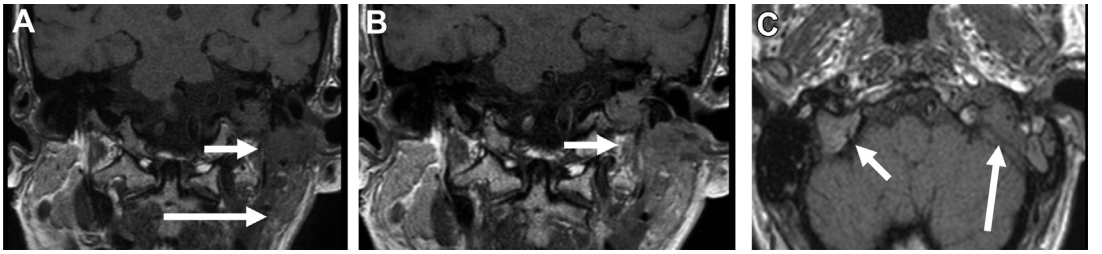

Fig. 16. Progressive SCCA due to inadequate treatment planning. Precontrast and postcontrast MR imaging were performed in a patient with an unknown primary tumor with extensive left-sided adenopathy which extended to the mastoid tip. The patient was treated with radiation therapy alone; however, the patient presented with progressive left neck pain. (*C*) Coronal noncontrast enhanced MR imaging shows a large low signal (*A*) enhancing mass (*B*) extending to the left skull base (*small arrow*) which has a higher signal compared with the adjacent parotid gland (*long arrow*). Axial images show diffuse replacement (*long arrow*) of the skull base compared to the contralateral side. These findings are consistent with a progressive tumor. These images were correlated with the treatment plan and the superior extent of the radiation did not include the mastoid tip with the superior extent of the field being between the long and short arrows on image A.

entities is crucial as management strategies differ completely. Both SCC and lymphoma arise from the same anatomic sites and show nearly similar imaging characteristics on conventional MR imaging sequences. On DWI, ADC is significantly lower in lymphoma (**Fig. 17**) than in SCC (**Fig. 18**) at primary or nodal sites, finding that is mostly attributed to higher cellularity in lymphoma. However, there is a greater possibility of overlap with the poorly differentiated SCCs, which tend to have a slightly lower ADC than their moderately or well-differentiated counterparts. Adding perfusion studies can help in the differentiation between these 2 pathologies. At DCE-MR, considering semiquantitative parameters derived from TIC, lymphoma shows longer TTP and lower enhancement peak than SCCs. Regarding quantitative assessment, several studies showed that lymphoma shows lower Ktrans and Ve values than SCC, which means that lymphoma shows less vascular permeability and tight extravascular extracellular space when compared with SCC. This reflects the histopathologic nature of lymphoma where there is high cellular density, few microvessels, and the tumor cells often form a sleeve-like infiltration around the vessels.[61,62]

Prediction Response to Therapy

Many studies have investigated the application of pretreatment ADC value for the prediction of outcome in patients with HN SCC. Tumors that show necrosis due to tumor hypoxia and decreased vascularity and have higher ADC values are less responsive to chemotherapy and radiotherapy. DWI can be used as a pretreatment marker for tumor hypoxia. Many studies suggested that higher pretreatment ADC values are predictive of poor local control and treatment

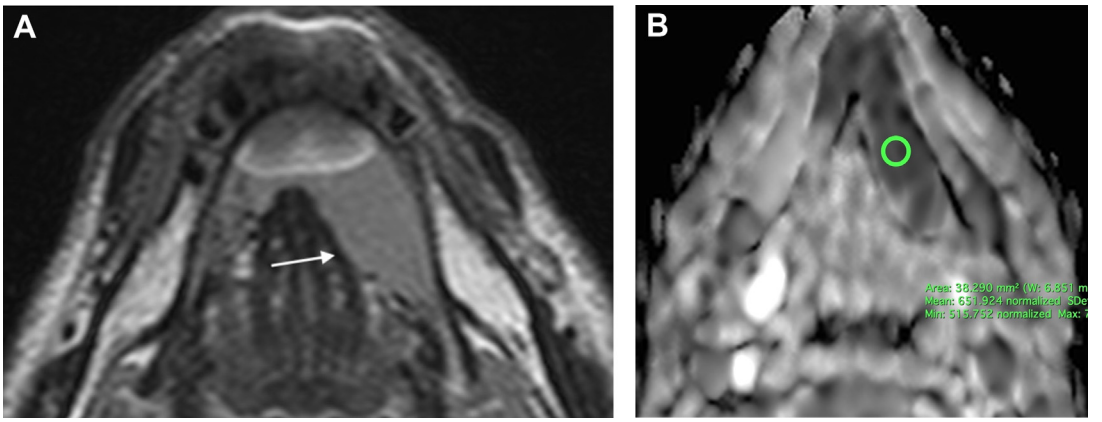

Fig. 17. Lingual lymphoma axial T2 and ADC map (*A*, *B*) showing left lingual lymphoma of intermediate signal intensity (*white arrow*) and ADC value 0.65 $\times$ 10^{-3} mm^2/s.

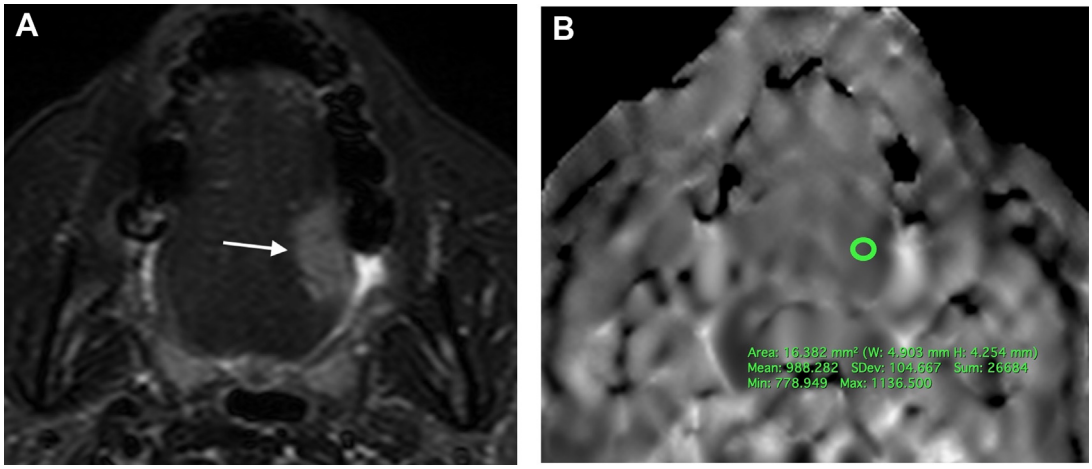

Fig. 18. Lingual SCC axial STIR and ADC map (*A, B*) showing left lingual SCC hyperintense to the muscle (*white arrow*) and ADC value 0.98 × 10^{-3} mm^2/s.

response. They found that an ADC greater than 1.15 × 10^{-3} mm^2/s in the primary tumor is associated with poor outcome after chemoradiation at 2-year follow-up.[7–12]

At DCE MR perfusion, low Ktrans value before the start of treatment, both in the primary tumor and the LN metastases, is associated with a worse prognosis, this could be explained as this lower permeability making it difficult for the chemotherapy agent to reach the cancer lesion. The role of DCE MR imaging metrics as predictors of response in HN cancers to conventional radiotherapy (CRT) and showed that HN cancer with higher pretreatment blood volume, and pretreatment Ktrans correlated with better response to CRT and disease-free survival. Tumors with higher blood flow and vascular permeability have better oxygenation with better access to CT and better response to RT.[22,34]

Intratreatment Assessment of Response to CRT

The efficacy of treatment is mainly evaluated by size changes of tumor and metastatic LNs before and after treatment. But actually, the size of the tumor will not change at the early stage, which makes it impossible to provide accurate information about the true response to treatment. As response adapted therapy becomes more widespread in cancer management, there will be greater interest in performing intratreatment scanning.[8–12]

DWI may help to closely monitor response in the early treatment phase and throughout treatment. Successful CRT results in rising in the ADC value in the first few weeks after the start of treatment. Some studies have shown that a smaller percentage of rising in the mean ADC value (<14–24%) in the first 3 weeks after the start of treatment is seen in patients with disease failure compared to those with disease control. In addition, it has been observed that after the initial early ADC rise, a subsequent ADC fall predicts locoregional failure, which may be caused by the repopulation of cancer cells.[12–15]

At DCE MR imaging perfusion, successful chemoradiotherapy causes changes in the time-intensity curve. Initially, there is a decrease in the number of leaking vessels, which is reflected as a slower rise of the enhancement curve. With continued successful response to therapy, there is a regression of tumor angiogenic properties resulting in a decreased contrast peak and the development of fibrosis resulting in a gradual accumulation of contrast. So, the TIC will change from rapid rise and ish-out in the pretreatment state to a slow rise and ish-in in the post-treatment state. In patients with poor response to CRT, TIC showed a steep rise in the enhancement curve, which means a high initial contrast peak value and a short TTP. This could help in identifying patients at risk of local recurrence as candidates for dose escalation or salvage surgery.[22] Results showed that the values of Ktrans and Kep significantly decreased, whereas Ve significantly increased after treatment, compared with those before treatment. Differences are statistically significant. Some studies have shown that radiochemotherapy will induce the deformation and necrosis of capillary walls, consequently reducing blood perfusion of tumor tissues, reducing osmotic pressure of the blood vessel walls, and decreasing values of Ktrans and Kep after radiochemotherapy. Ve value increases maybe because the radiotherapy leads to osmotic pressure decreases of the tumor vessel walls, slows the flow rate of contrast agents, prolongs the

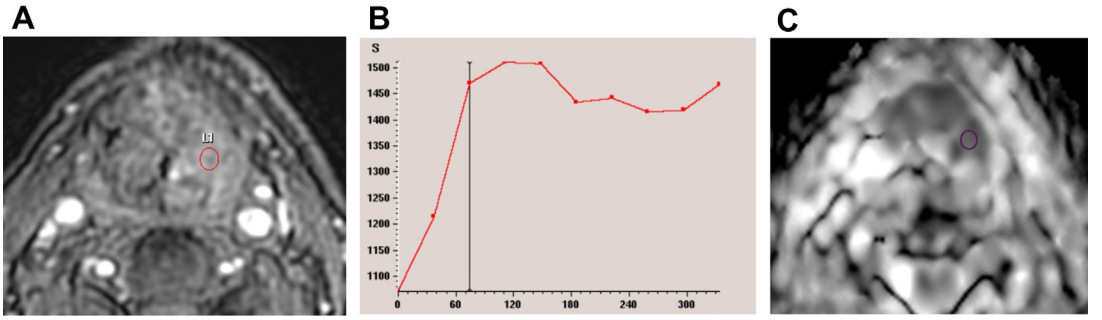

Fig. 19. Recurrent supraglottic SCC. Patient with left recurrent supraglottic SCC after management by chemoradiotherapy. DCE sequence and regenerated curve (*A*, *B*) show nodular enhancing left supraglottic mass with rapid enhancement followed by a gradual wash-out confirming its malignant nature. ADC map (*C*) showing hypointense signal of the lesion; ADC value 0.9 $\times$ 10^{-3} mm^2/s.

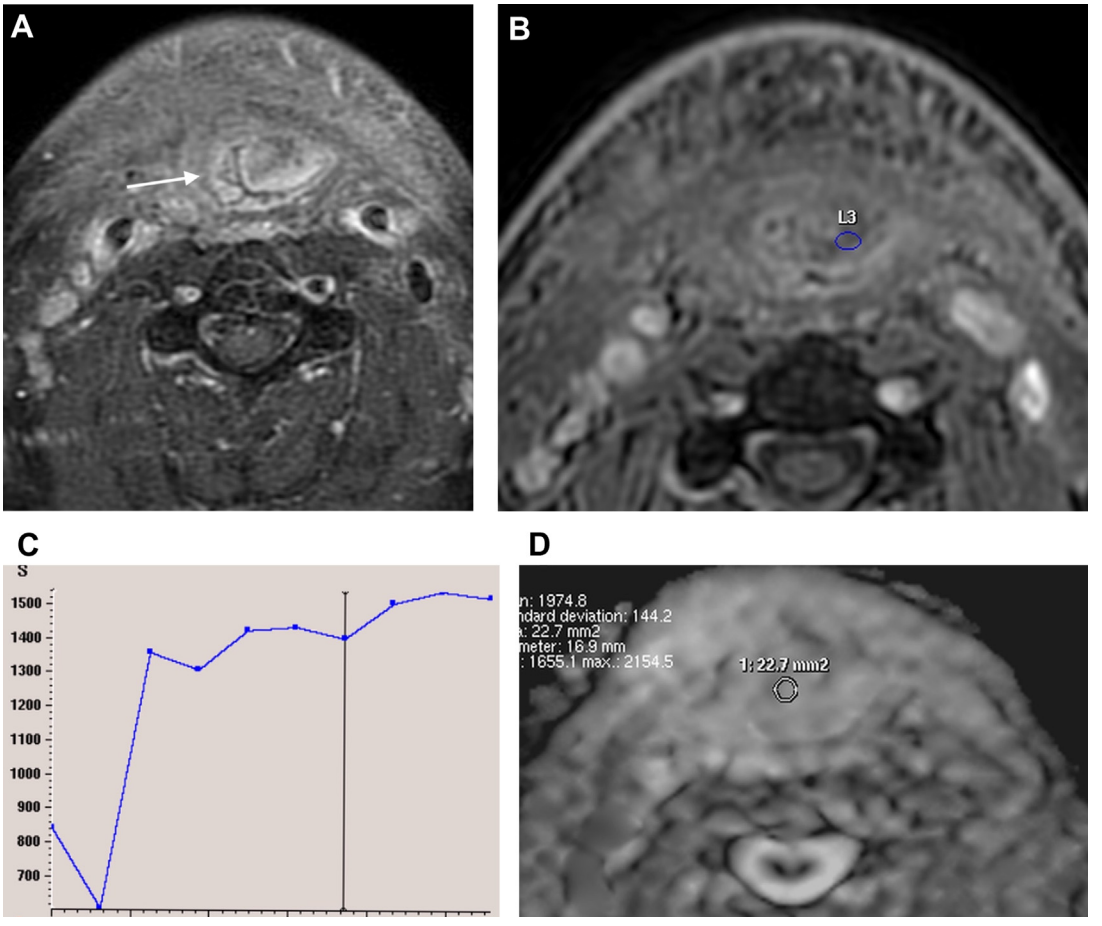

Fig. 20. Postradiation changes. Patient with laryngeal SCC managed by total laryngectomy and chemoradiotherapy. Axial T1 postcontrast fat-saturated image (*A*) showing diffuse thin linear enhancement of the mucosa of the reconstructed neopharynx and submucosal edema (*white arrow*). In the DCE sequence and regenerated curve (*B*, *C*), the curve shows rapid enhancement followed by a continuous regular rising curve representing benignity. ADC map (*D*) shows a high signal intensity of the reconstructed neopharynx ADC value 1.22 $\times$ 10^{-3} mm^2/s representing postirradiation inflammation and edema.

residence time of contrast agents in the tissue vessels and outside the vascular, and eventually leads to an increase of Ve values.[8–13]

Recurrence Versus Postradiation Changes

The baseline scan is typically obtained at 8 to 10 weeks after chemoradiation, whereas postsurgical scans are often obtained around 10 to 12 weeks. The baseline cross-sectional scan serves as a "road map" of a deformed neck to increase sensitivity for early recurrent disease on the subsequent surveillance imaging. For this reason, it is ideal that the same cross-sectional modality chosen for baseline imaging, either CT or MR, is subsequently used for surveillance. Follow-up may be performed in 3 to 6 months intervals, depending on the initial tumor staging and histologic prognostic features and the ongoing clinical course and physical findings. At any follow-up imaging examination, the possibility of a second primary tumor must again be considered. Remember on every follow-up study to look for residual, recurrent, and new tumors.[8–13] Radiation with or without chemotherapy is associated with significant changes in the appearance of neck soft tissues. Radiation results in acute inflammation of all tissues in the radiation field with extensive edema. Over time this converts to fibrosis with atrophy and altered signal intensity and texture on MR. Both acute and chronic expected radiation changes can be confusing on CT or MR, requiring careful evaluation and comparison with prior studies to detect early recurrences.[7–11]

On MR imaging, the recurrent tumors will have similar signal characteristics to the primary tumor, so it is important to review any preoperative imaging if available. A new nodule within the tumor bed or progressive thickening of the tissues deep to the flap is a concerning feature for recurrent disease. T2 sequences are useful to distinguish scar from a tumor, with scar tissue being of comparatively lower signal on T2. Several previous studies have reported that the imaging criteria for local tumor recurrence include an infiltrative mass, intermediate T1-weighted signal intensity, intermediate to high T2-weighted signal intensity, and enhancement. However, differentiating residual or recurrent tumor from scar using these imaging criteria is difficult because these findings could overlap with those for post-treatment edematous change, radiation-induced inflammation, or fibrosis. Quantitative analysis of diffusion MR imaging metrics can help distinguish between residual/recurrent malignant tissue and benign post-treatment changes. Prior studies suggested that residual HNSCC tends to have a lower average ADC compared with benign post-treatment changes (see **Fig. 2**). The suggested ADC thresholds in different studies for differentiating residual/recurrent (**Fig. 19**) malignant tissue

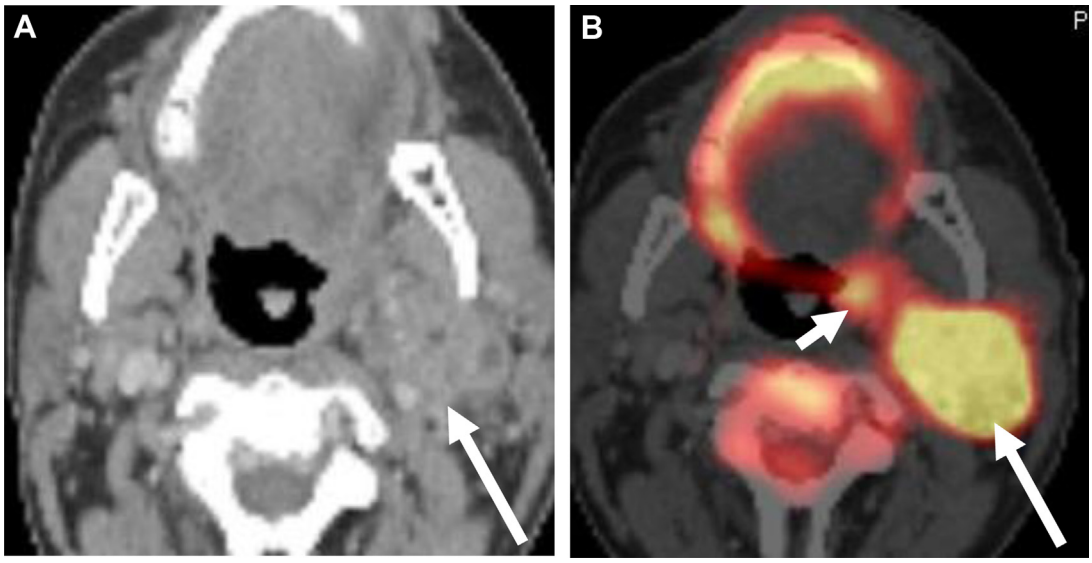

Fig. 21. Unknown primary detected with PET-CT. (*A*) Axial contrast-enhanced CT shows a large left level II nodal mass which was biopsy-proven SCC (*arrow*). No tumor was identified on direct endoscopy. The patient was thought to have an unknown primary and underwent PET-CT in an attempt to localize the tumor and help direct speculative biopsies. (*B*) PET-CT shows uptake in the large left nodal mass (*long arrow*) and focal uptake in the left tonsil (*small arrow*), which was suspicious for a left tonsillar carcinoma. The patient underwent a left tonsillectomy, which confirmed the diagnosis of a left tonsillar carcinoma, which was initially felt to be an unknown primary cancer eventually detected by PET-CT.

and benign post-treatment changes (Fig. 20) varied from 0.96 to 1.46 $\times$ 10^{-3} mm^2/s. These findings are likely reflective of the difference in cellularity of malignant tissue compared to fibrotic post-treatment changes. At DCE MR imaging, a rapid wash-in followed by a wash-out or plateau phase is indicative of tumor, while slowly progressive enhancements indicate benign post-treatment changes.[62–68]

Unknown Primary

An unknown primary tumor is defined as SCC detected from fine-needle aspiration of a nodal mass in the absence of a clinically evident primary source. More than 90% of unknown primary tumors are determined to be HPV-related OPSCC. As HPV-related tumors arise from the palatine tonsils and base of the tongue, it is essential to evaluate CT and MR scan for subtle asymmetry in the size and signal intensity to identify the primary lesion and direct surgeons to biopsy or tonsillectomy. PET-CT is often performed in the United States to help direct speculative biopsies and possibly identify the primary site in patients with metastatic LNs and negative endoscopy (Fig. 21). Determination of the true primary can markedly limit the radiation field used for therapy. High temporal resolution (ultrafast) DCE MR imaging has been found to improve the detection of clinically occult primary tumors in patients presenting with cervical SCC LN metastases. Qualitative reading of ultrafast-DCE images could depict early intensity changes and faster signal enhancement as indications for malignancy compared with normal tissue.[69]

SUMMARY

Routine and advanced MR imaging sequences are used for locoregional spread, nodal, and distant staging, aids treatment planning, predicts treatment response, differentiates recurrence for post-radiation changes, and monitor patients after chemoradiotherapy.

CLINICS CARE POINTS

- MRI helps asses soft tissue spread and provides better tumor characterization compared to MR.
- MRI is the study of choice for evaluating perineural spread.
- Advanced MRI techniques may be helpful to differentiate recurrent tumor from post-treatment changes.

REFERENCES

1. Chow LQM. Head and Neck Cancer. N Engl J Med 2020;382:60–72.
2. Argiris A, Karamouzis MV, Raben D, et al. Head and neck cancer. Lancet 2008;371:1695–709.
3. Pfister DG, Spencer S, Adelstein D, et al. Head and Neck Cancers, Version 2.2020, NCCN Clinical Practice Guidelines in Oncology. J Natl Compr Canc Netw 2020;18:873–98.
4. Lydiatt WM, Patel SG, O'Sullivan B, et al. Head and Neck cancers-major changes in the American Joint Committee on cancer eighth edition cancer staging manual. CA Cancer J Clin 2017;67:122–37.
5. Machiels JP, René Leemans C, Golusinski W, et al. Squamous cell carcinoma of the oral cavity, larynx, oropharynx and hypopharynx: EHNS-ESMO-ESTRO Clinical Practice Guidelines for diagnosis, treatment and follow-up. Ann Oncol 2020;31:1462–75.
6. Junn JC, Soderlund KA, Glastonbury CM. Imaging of Head and Neck Cancer With CT, MRI, and US. Semin Nucl Med 2021;51:3–12.
7. Glastonbury CM. Head and neck squamous cell cancer: approach to staging and surveillance. 2020. In: Hodler J, Kubik-Huch RA, von Schulthess GK, editors. Diseases of the brain, head and neck, spine 2020–2023.
8. Abdel Razek AA. Computed tomography and magnetic resonance imaging of lesions at masticator space. Jpn J Radiol 2014;32:123–37.
9. El Beltagi AH, Elsotouhy AH, Own AM, et al. Functional magnetic resonance imaging of head and neck cancer: Performance and potential. Neuroradiol J 2019;32:36–52.
10. Santos Armentia E, Martín Noguerol T, Suárez Vega V. Advanced magnetic resonance imaging techniques for tumors of the head and neck. Radiologia 2019;61:191–203.
11. Abdel Razek AA. Imaging of connective tissue diseases of the head and neck. Neuroradiol J 2016;29:222–30.
12. Juliano A, Moonis G. Computed Tomography Versus Magnetic Resonance in Head and Neck Cancer: When to Use What and Image Optimization Strategies. Magn Reson Imaging Clin N Am 2018;26:63–84.
13. Razek AA, Castillo M. Imaging appearance of granulomatous lesions of head and neck. Eur J Radiol 2010;76:52–60.
14. Seeburg DP, Baer AH, Aygun N. Imaging of Patients with Head and Neck Cancer: From Staging to Surveillance. Oral Maxillofac Surg Clin North Am 2018;30:421–33.
15. Abdel Razek AA. Assessment of solid lesions of the temporal fossa with diffusion-weighted magnetic resonance imaging. Int J Oral Maxillofac Surg 2015;44:1081–5.

16. Thoeny HC, De Keyzer F, King AD. Diffusion-weighted MR imaging in the head and neck. Radiology 2012;263:19–32.
17. Abdel Razek AA, Nada N. Role of diffusion-weighted MRI in differentiation of masticator space malignancy from infection. Dentomaxillofac Radiol 2013; 42:20120183.
18. Abdel Razek A, Mossad A, Ghonim M. Role of diffusion-weighted MR imaging in assessing malignant versus benign skull-base lesions. Radiol Med 2011;116:125–32.
19. Abdel Razek AAK. Routine and Advanced Diffusion Imaging Modules of the Salivary Glands. Neuroimaging Clin N Am 2018;28:245–54.
20. Khalek Abdel Razek AA. Characterization of salivary gland tumours with diffusion tensor imaging. Dentomaxillofac Radiol 2018;47:20170343.
21. Ma G, Xu XQ, Hu H, et al. Utility of Readout-Segmented Echo-Planar Imaging-Based Diffusion Kurtosis Imaging for Differentiating Malignant from Benign Masses in Head and Neck Region. Korean J Radiol 2018;19:443–51.
22. Kabadi SJ, Fatterpekar GM, Anzai Y, et al. Dynamic Contrast-Enhanced MR Imaging in Head and Neck Cancer. Magn Reson Imaging Clin N Am 2018;26: 135–49.
23. Razek AA, Elsorogy LG, Soliman NY, et al. Dynamic susceptibility contrast perfusion MR imaging in distinguishing malignant from benign head and neck tumors: a pilot study. Eur J Radiol 2011;77:73–9.
24. Abdel Razek AA, Samir S, Ashmalla GA. Characterization of Parotid Tumors With Dynamic Susceptibility Contrast Perfusion-Weighted Magnetic Resonance Imaging and Diffusion-Weighted MR Imaging. J Comput Assist Tomogr 2017;41:131–6.
25. Abdel Razek AAK, Talaat M, El-Serougy L, et al. Clinical Applications of Arterial Spin Labeling in Brain Tumors. J Comput Assist Tomogr 2019;43:525–32.
26. Abdel Razek AAK, Nada N. Arterial spin labeling perfusion-weighted MR imaging: correlation of tumor blood flow with pathological degree of tumor differentiation, clinical stage and nodal metastasis of head and neck squamous cell carcinoma. Eur Arch Otorhinolaryngol 2018;275:1301–7.
27. Razek AAKA. Multi-parametric MR imaging using pseudo-continuous arterial-spin labeling and diffusion-weighted MR imaging in differentiating subtypes of parotid tumors. Magn Reson Imaging 2019;63:55–9.
28. Abdel Razek AA, Poptani H. MR spectroscopy of head and neck cancer. Eur J Radiol 2013;82:982–9.
29. Abdel Razek AAK. Editorial for "Preliminary Assessment of Intravoxel Incoherent Motion Diffusion-Weighted MRI (IVIM-DWI) Metrics in Alzheimer's Disease. J Magn Reson Imaging 2020;52:1827–8.
30. Razek AAKA. Editorial for "Preoperative MRI-Based Radiomic Machine-Learning Nomogram May Accurately Distinguish Between Benign and Malignant Soft Tissue Lesions: A Two-Center Study. J Magn Reson Imaging 2020;52:883–4.
31. Abdel Razek AAK, Gadelhak BN, El Zahabey IA, et al. Diffusion-weighted imaging with histogram analysis of the apparent diffusion coefficient maps in the diagnosis of parotid tumours. Int J Oral Maxillofac Surg 2021. https://doi.org/10.1016/j.ijom.2021.03.019.
32. Glastonbury CM. Critical Changes in the Staging of Head and Neck Cancer. Radiol Imaging Cancer 2020;2:e190022.
33. Glastonbury CM, Mukherji SK, O'Sullivan B, et al. Setting the Stage for 2018: How the Changes in the American Joint Committee on Cancer/Union for International Cancer Control Cancer Staging Manual Eighth Edition Impact Radiologists. AJNR Am J Neuroradiol 2017;38:2231–7.
34. Yousem D, Gad K, Tufano R. Resectability Issues with Head and Neck Cancer. AJNR Am J Neuroradiol 2006;27:2024–36.
35. Lydiatt W, O'Sullivan B, Patel S. Major Changes in Head and Neck Staging for 2018. Am Soc Clin Oncol Educ Book 2018;38:505–14.
36. Huopainen P, Jouhi L, Hagstrom J, et al. MRI correlates to histopathological data in oral tongue squamous cell carcinoma diagnostics. Acta Odontol Scand 2021;79:161–6.
37. Cho SJ, Lee JH, Suh CH, et al. Comparison of diagnostic performance between CT and MRI for detection of cartilage invasion for primary tumor staging in patients with laryngo-hypopharyngeal cancer: a systematic review and meta-analysis. Eur Radiol 2020;30:3803–12.
38. Kuno H, Sakamaki K, Fujii S, et al. Comparison of MR Imaging and Dual-Energy CT for the Evaluation of Cartilage Invasion by Laryngeal and Hypopharyngeal Squamous Cell Carcinoma. AJNR Am J Neuroradiol 2018;39:524–31.
39. Ogawa T, Kojima I, Wakamori S, et al. Clinical utility of apparent diffusion coefficient and diffusion-weighted magnetic resonance imaging for resectability assessment of head and neck tumors with skull base invasion. Head Neck 2020;42:2896–904.
40. Lee YC, Jung AR, Kwon OE, et al. Comparison of Computed Tomography, Magnetic Resonance Imaging, and Positron Emission Tomography and Computed Tomography for the Evaluation Bone Invasion in Upper and Lower Gingival Cancers. J Oral Maxillofac Surg 2019;77:875.e1-9.
41. Meerwein CM, Pizzuto DA, Vital D, et al. Use of MRI and FDG-PET/CT to predict fixation of advanced hypopharyngeal squamous cell carcinoma to prevertebral space. Head Neck 2019;41:503–10.
42. Tian D, Huang H, Yang YS, et al. Depth of Invasion into the Circular and Longitudinal Muscle Layers in T2 Esophageal Squamous Cell Carcinoma Does Not Affect Prognosis or Lymph Node Metastasis: A

Multicenter Retrospective Study. World J Surg 2020; 44:171–8.
43. Wang JC, Takashima S, Takayama F, et al. Tracheal invasion by thyroid carcinoma: prediction using MR imaging. AJR Am J Roentgenol 2001;177:929–36.
44. Spector ME, Gallagher KK, McHugh JB, et al. Correlation of radiographic and pathologic findings of dermal lymphatic invasion in head and neck squamous cell carcinoma. AJNR Am J Neuroradiol 2012;33:462–4.
45. Nemec SF, Linecker A, Czerny C, et al. Detection of cutaneous invasion by malignant head and neck tumors with MDCT. Eur J Radiol 2008;68:335–9.
46. Agarwal M, Wangaryattawanich P, Rath TJ. Perineural Tumor Spread in Head and Neck Malignancies. Semin Roentgenol 2019;54:258–75.
47. Dankbaar JW, Pameijer FA, Hendrikse J, et al. Easily detected signs of perineural tumour spread in head and neck cancer. Insights Imaging 2018;9:1089–95.
48. Abdel Razek AA, Gaballa G. Role of perfusion magnetic resonance imaging in cervical lymphadenopathy. J Comput Assist Tomogr 2011;35:21–5.
49. Razek AAKA, Helmy E. Multi-parametric arterial spin labeling and diffusion-weighted imaging in differentiation of metastatic from reactive lymph nodes in head and neck squamous cell carcinoma. Eur Arch Otorhinolaryngol 2021;278:2529–35.
50. Pons Y, Ukkola-Pons E, Clément P, et al. Relevance of 5 different imaging signs in the evaluation of carotid artery invasion by cervical lymphadenopathy in head and neck squamous cell carcinoma. Oral Surg Oral Med Oral Pathol Oral Radiol Endod 2010;109:775–8.
51. Yousem DM, Hatabu H, Hurst RW, et al. Carotid artery invasion by head and neck masses: prediction with MR imaging. Radiology 1995;195:715–20.
52. Razek AA, Tawfik A, Rahman MA, et al. Whole-body diffusion-weighted imaging with background body signal suppression in the detection of osseous and extra-osseous metastases. Pol J Radiol 2019;84: e453–8.
53. Razek AAKA, Shamaa S, Lattif MA, et al. Interobserver agreement of whole-body computed tomography in staging and response assessment in lymphoma: the lugano classification. Pol J Radiol 2017;82:441–7.
54. Razek AA, Nada N. Correlation of choline/creatine and apparent diffusion coefficient values with the prognostic parameters of head and neck squamous cell carcinoma. NMR Biomed 2016;29:483–589.
55. Javadi S, Menias CO, Karbasian N, et al. HIV-related Malignancies and Mimics: Imaging Findings and Management. Radiographics 2018;38:2051–68.
56. Payabvash S, Chan A, Jabehdar, et al. Quantitative diffusion magnetic resonance imaging for prediction of human papillomavirus status in head and neck squamous-cell carcinoma: A systematic review and meta-analysis. Neuroradiol J 2019;32(4):232–40.
57. Abdel Razek AA, Kamal E. Nasopharyngeal carcinoma: correlation of apparent diffusion coefficient value with prognostic parameters. Radiol Med 2013;118:534–9.
58. Abdel Razek AA, Elkhamary S, Al-Mesfer S, et al. Correlation of apparent diffusion coefficient at 3T with prognostic parameters of retinoblastoma. AJNR Am J Neuroradiol 2012;33:944–8.
59. Abdel Razek AAK, Elkhamary SM, Nada N. Correlation of apparent diffusion coefficient with histopathological parameters of salivary gland cancer. Int J Oral Maxillofac Surg 2019;48:995–1000.
60. Razek AA. Diffusion-weighted magnetic resonance imaging of head and neck. J Comput Assist Tomogr 2010;34:808–15.
61. Bae S, Choi YS, Sohn B, et al. Squamous Cell Carcinoma and Lymphoma of the Oropharynx: Differentiation Using a Radiomics Approach. Yonsei Med J 2020;61:895–900.
62. Eissa L, Abdel Razek AAK, Helmy E. Arterial spin labeling and diffusion-weighted MR imaging: Utility in differentiating idiopathic orbital inflammatory pseudotumor from orbital lymphoma. Clin Imaging 2021;71:63–8.
63. Chung SR, Choi YJ, Suh CH, et al. Diffusion-weighted Magnetic Resonance Imaging for Predicting Response to Chemoradiation Therapy for Head and Neck Squamous Cell Carcinoma: A Systematic Review. Korean J Radiol 2019;20:649–61.
64. Abdel Razek AAK, Abdelaziz TT. Neck Imaging Reporting and Data System: What Does Radiologist Want to Know? J Comput Assist Tomogr 2020;44: 527–32.
65. Abdelaziz TT, Abdel Razk AAK, Ashour MMM, et al. Interreader reproducibility of the Neck Imaging Reporting and Data system (NI-RADS) lexicon for the detection of residual/recurrent disease in treated head and neck squamous cell carcinoma (HNSCC). Cancer Imaging 2020;20:61.
66. Abdel Razek AAK. Arterial spin labelling and diffusion-weighted magnetic resonance imaging in differentiation of recurrent head and neck cancer from post-radiation changes. J Laryngol Otol 2018; 132:923–8.
67. Abdel Razek AA, Gaballa G, Ashamalla G, et al. Dynamic Susceptibility Contrast Perfusion-Weighted Magnetic Resonance Imaging and Diffusion-Weighted Magnetic Resonance Imaging in Differentiating Recurrent Head and Neck Cancer From Postradiation Changes. J Comput Assist Tomogr 2015;39:849–54.
68. Razek AAKA. Diffusion tensor imaging in differentiation of residual head and neck squamous cell carcinoma from post-radiation changes. Magn Reson Imaging 2018;54:84–9.
69. Donta TS, Smoker WR. Head and neck cancer: carcinoma of unknown primary. Top Magn Reson Imaging 2007;18:281–92.